A Machine Learning Approach to Decipher the Origin of Magnetic Anisotropy in Three-Coordinate Cobalt Single-Ion Magnets

Rajanikanta Rana, Abinash Swain, Garima Bangar and Gopalan Rajaraman*

Department of Chemistry, Indian Institute of Technology Bombay, Mumbai-400076, India. email: rajaraman@chem.iitb.ac.in).

Abstract

Single Molecule Magnets (SMMs) emulate permanent magnets and are highly regarded for their role in compact information storage and molecular spintronics. Their behavior is primarily governed by magnetic anisotropy, expressed through parameters like the axial zero-field splitting (D) and orientation of magnetic anisotropy (gx, gy, gz) in mononuclear transition metal complexes. Low-coordinate mononuclear transition metal complexes stand out for their substantial anisotropy and higher blocking temperatures. However, understanding the intricate interplay between these parameters poses a significant challenge, often beyond traditional magneto-structural correlations. Hence, machine learning (ML) tools have been embraced to address these complexities. By employing an ML model based on Co-ligand bond length and angle relative to the pseudo-C3 axis, this study effectively rationalizes variations in D values, g-factors, and rhombic anisotropy, crucial for determining magnetic properties. Leveraging a dataset of 627 molecules, the research explores ML's potential in predicting magnetic anisotropy parameters in three-coordinate Co(II) complexes, achieving a minimal mean absolute error (MAE) of approximately 17 cm^{-1} and high accuracy levels exceeding 95% for classification tasks. These insights offer valuable guidance for the development of innovative single-ion magnets.

Introduction

Mimicking the principle of super-paramagnetism behaviour by molecules at the electronic levels can be the potential future alternative for bulk nanomagnetic materials[1]. The class of molecules for which these phenomena are observed are called Single Molecule Magnets (SMMs)[2], where the magnetisation can be frozen after removing the magnetic field below the blocking temperatures (T_B). Lanthanides dominated the last decade in this area, but they have several disadvantages, such as (i) abundancy and cost, (ii) difficulty in controlling the geometry around the metal ion due to large coordination number, (iii) retaining properties on surfaces, (iv) challenges in controlling the spin Hamiltonian parameters.[3] Among several alternative avenues available, first-row transition metal-ion-based single-ion magnets (SIMs) top the list as many of the aforementioned problems can be tackled.[4-6] For the SMMs with transition metal ions, the performance primarily depends on the barrier of spin reversal (U_{eff}), which in turn is governed by the axial zero-field splitting parameter (*zfs*; D), the rhombic anisotropy (E/D), orientation of magnetic axis which depends on g_x, g_y, g_z and quantum tunneling of magnetisation.[6] Based on the relationship $U_{eff} = S|D|^2$, (where S is an integer spin), a large axial zero-field splitting (D) with a large spin ground state S yields a large U_{eff} value. However, concurrently achieving both a large spin state S and a large D value is unlikely, as these two parameters antagonise each other in multinuclear systems.[7,8] As the *zfs* parameters, axial and rhombic anisotropy can be viably controlled in mononuclear transition metal complexes, several successful attempts have been made to synthesise novel SIMs based on mononuclear complexes. This includes but is not limited to a (i) report of two coordinate Co SIMs with a record high U_{eff} value of 450 cm^{-1}, (ii) report of Ni(II) complexes exhibiting a record high D of 399 cm^{-1}, (iii) report of two-coordinate Fe(I) exhibiting U_{eff} of 226 cm^{-1}.[9-11] If we look closely at all these examples, it is clear that to obtain a large *zfs* parameter one needs (i) unquenched angular momentum that often occurs when the coordination number is relatively small (one to three), (ii) have more than half-filled d-electronic configuration and (iii) preferably a Kramers ground state to avoid ground state quantum tunnelling effects.[6,12-14]

Among the first-row elements that satisfy many of the above criteria is the Cobalt ion. While two-coordinate Co systems are attractive, only a few examples are reported as these are synthetically challenging.[14,38,39] An ideal four-coordinate Co complex losses anisotropy due to the adaption of tetrahedral geometry, therefore, the midground is three-coordinate Co complexes as the ligand field is still not sufficiently high to quench the orbital contributions.

The highest pseudo symmetry point group of D_{3h} or C_{3v} in this class of molecules has a unique principle axis which can generate magnetic anisotropy. A quick Cambridge structural database search reveals a report of 140 three-coordinate Co complexes with various donor atoms exemplifying the versatility, [40,41] Although there are several correlations and design clues offered for various Co SIMs with a coordination number starting from four[14], to the best of our knowledge, such an endeavour is missing for three coordinate Co complexes, despite its potential.

Exploring magnetic anisotropy involves a combination of experimental and computational approaches. In the realm of computational methods, despite significant progress, accurately determining magnetic anisotropy remains a formidable task.[15-17] Density functional theory (DFT) frequently encounters challenges [18,19], affirming Griffith's theory [c] that spin-orbit couplings play a substantial role in influencing zero-field splitting (ZFS) in transition metals. Consequently, chemists turn to complex techniques such as complete-active-space self-consistent field (CASSCF) and multireference configuration interaction, which demand substantial computational resources. In recent years, the swift evolution of machine-learning (ML) methods has raised the prospect of revolutionizing diverse aspects of human society. This potential stems from the proven ability of ML models, provided they have a sufficient number of neurons and access to ample data, to approximate any given function[20,21]. While still in its early stages, the fields of molecular and materials science are already reaping the rewards of scientific machine learning (ML) in various applications, including areas like energetics [22,23] and molecular dynamics.[24] While applications in the field of multiscale molecular magnetism are not yet widespread, recent efforts have started to establish initial methodologies for tackling the intricacies of the spin Hamiltonian[25], spin dynamics[26], and spin-phonon coupling across extensive clusters.[27] There have also been endeavors to characterize the dynamic g and anisotropic tensors in vibronically active systems.[28-30]

Theoretical tools particularly, based on CASSCF in combination with effective Hamiltonian approach (EHA) proven to an invaluable tool to obtain sign and magnitude of D value with good numerical accuracy and chemical insights.[31,32] However, utilising these tools for prediction pose a significant challenge as they demand high-computational cost and therefore cannot used as a screening tool.[21,33] The AI/ML approach has been demonstrated recently for spin state of spin crossover systems and exchange coupling in transition metal complexes.[34,35] For spin crossover systems using artificial neural networks (ANN) with a high percentage of

.i.e. >95% correct spin state assignments. For unconventional spin-crossover complexes, a genetic algorithm (GA) optimization combined with an ANN was used.[36,37]

With our team's substantial proficiency in molecular magnetism, developed through the utilization of DFT and multi-reference *ab initio* calculations, our objective here is to assess the potential of adopting a machine-learning (ML) approach to precisely extract the axial magnetic anisotropy component (D), rhombic anisotropy, effective g-factors and quantum tunneling of magnetization(QTM) which can be derived from effective spin Hamiltonian (equation 1). In the context of the expression for $\widehat{H}$ (zfs), the parameter E represents the rhombic distortion in the zero-field splitting tensor, which denotes the deviation from axial symmetry. When E is zero, the system exhibits axial symmetry, and the anisotropy tensor is described as purely axial. Conversely, a non-zero E introduces a rhombic distortion, providing crucial information about the asymmetry in the electronic environment of the magnetic center. Understanding the significance of E is essential for interpreting the magnetic properties and behaviors in systems with anisotropic electron distributions. This endeavor centered on establishing correlations between structural parameters and the multi-reference CASSCF D values, with the intention of alleviating the complexities linked to the use of multi-reference methods.

$$\widehat{H}_{zfs} = D\left[\hat{s}_z^2 - \frac{1}{3}s(s+1)\right] + E(\hat{s}_x^2 - \hat{s}_y^2)$$

Eqn. (1)

If Z is the main anisotropy axis, the axial parameter ZFS D is defined as,

$$D = D_{ZZ} - \frac{1}{2}(D_{XX} - D_{YY})$$

The Rhombic ZFS parameter E is then defined $E = \frac{1}{2}(D_{XX} - D_{YY})$

The main anisotropy axis is chosen so that the D_{ZZ} value differs most from the D_{XX} and D_{YY} ones. For our study, we compiled an extensive CASSCF data, encompassing the geometric and electronic characteristics of Co^{II} Single Ion Magnets (SIMs). Among the 140 examples reported, we have chosen all possible combinations in terms of donor atoms of Co^{II} and derive 538 model structures to perform *ab initio* CASSCF calculations using ORCA 5.0.4[27] package (see computational details in ESI). This has been carried out to obtain insights into how the *zfs* parameter varies with respect to the nature of donor atoms (soft vs hard donor ligands), structural distortions/fluctuations.

Machine Learning Models:

We've chosen four prominent machine learning models to predict D, E/D and g_x, g_y and g_z: Gradient Boosting Regression (GBR), Random Forest Regression (RFR), Decision Tree Regression (DTR), and Kernel Ridge Regression (KRR)[42]. Additionally, eight distinct machine learning algorithms were utilized for predicting the sign of D. These algorithms include Logistic Regression (LR)[43], k-Nearest Neighbors (KNN)[44], Support Vector Machine (SVM)[45], Decision Tree (DT)[46], Random Forest (RF)[47], Adaptive Boosting (AD)[48], Gradient Boosting (GB)[49], and Multilayer Perceptron (MLP)[50]. All models were implemented in Python using the scikit-learn package.[47] We optimized hyperparameters and mitigated overfitting with 5-fold grid-search cross-validation, repeating the process five times with random dataset splits to counter sampling bias. Evaluation metrics are based on the average prediction results, as depicted in Figure **S1**.

Results

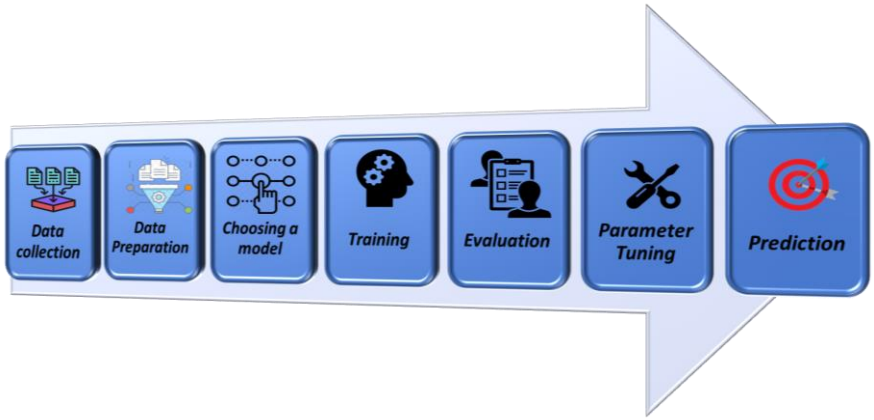

Figure **1**. Illustrates the predictive process for CASSCF computed spin Hamiltonian parameters with the aid of machine learning models.

Initially, we curated around 90 tri-coordinated Co (II) complexes from existing literature. To expand our dataset, we conducted optimizations, introducing ligand modifications. And hence we expand our sample size to 627 molecules. Within this dataset, we made predictions for D values, E/D parameters, and g-factors. Out of the 627 data points, 395 had a positive D, while 232 had a negative D. The D values spanned from 110 to -206 cm^{-1}, E/D ranged from 0.00001

to 0.33, and gzz varied from 2.06 to 4.08. For classification purposes, we assign a category of 1 to D values with a positive sign and 0 to D values with a negative sign.

To begin, we pinpointed a set of 7 descriptors that likely influence both the sign and magnitude of D. These descriptors encompass structural parameters, namely bond angles and bond lengths. Specifically, we considered the bond lengths associated with the Co atom and the atoms within the first coordination sphere, yielding three bond lengths (BL1, BL2, BL3). For consistency in our datasets, we arranged these bond lengths in ascending order as BL1 < BL2 < BL3.

Similarly, we extended this approach to bond angles, establishing a sequence where BA1 < BA2 < BA3. Additionally, we introduced a new parameter, ϕ, which quantifies the root-mean-square displacement (RMSD) of atomic coordinates from an ideal $\{CoX_3\}$ core possessing C_{3v} point group; see ESI for details[45]. This collective set of descriptors amounts to 7 structural parameters. Subsequently, we took the dataset, consisting of a total of 627 complexes characterized by these 7 descriptors, and subjected it to a random shuffling. Following this, we divided the shuffled dataset into two segments: a training dataset (80%) and a test dataset (20%) for predictions.

Machine Learning Models to Predict the ZFS (D)

In pursuit of our objective, we selected four prominent ML models: GradientBoost regression (GBR), random forest regression (RFR), decision tree regression (DTR), and kernel ridge regression (KRR). To optimize model performance, we rigorously fine-tuned hyperparameters using gridSearchCV (see Table S1). We evaluated model performance by calculating the mean absolute error (MAE) on the test dataset, employing an 80% training and 20% test data split. The GBR model emerged as the best-fitted model with a minimal test MAE of approximately 17 cm^{-1}, boasting the highest accuracy among all models (Table S2). This competitive edge may stem from GBR's proficiency in identifying optimal node splits for parallel regression trees. To ensure the stability and generalization of the Gradient Boosting (GB) model, we conducted a 5-fold cross-validation, as detailed in Table S3. The accuracy values for each fold closely matched the test accuracy, indicating the model's stability. The scatter plot (Figure 2a) illustrated the model's generalizability and transferability, showcasing robust predictions for both the training and test sets. Further, we assessed dataset uniformity through train-test splits at various ratios (80:20, 70:30, 60:40, and 50:50), as presented in Table S4. Consistent test accuracy across different splits confirmed dataset uniformity. To mitigate human bias in test

set selection, the procedure was iterated a hundred times with distinct train and test sets controlled by a seed value. The reported test R2 represents the average R2 across these runs, addressing model performance variability and bolstering assessment robustness (See ESI fig S2).

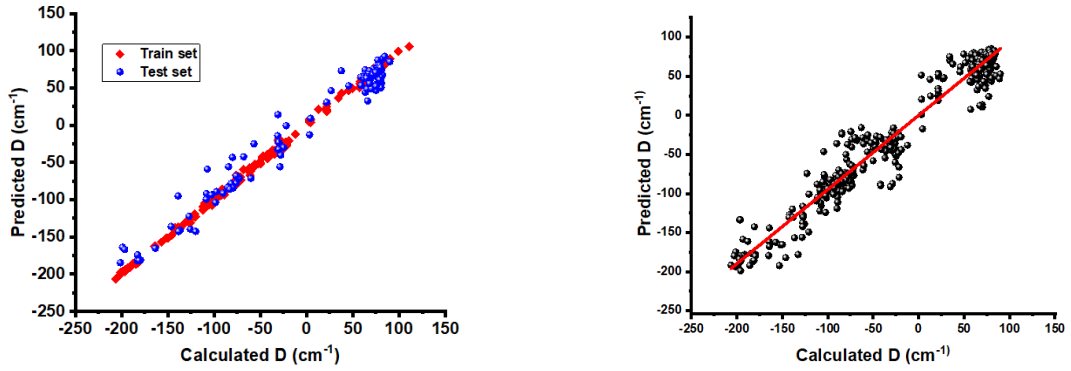

Figure 2. (a) Scatter plots illustrate the comparison between ML-predicted and CASSCF-calculated D values within both training and testing datasets. (b) Predicted vs CASSCF calculated D from 5-fold cross-validation using gradient boosting

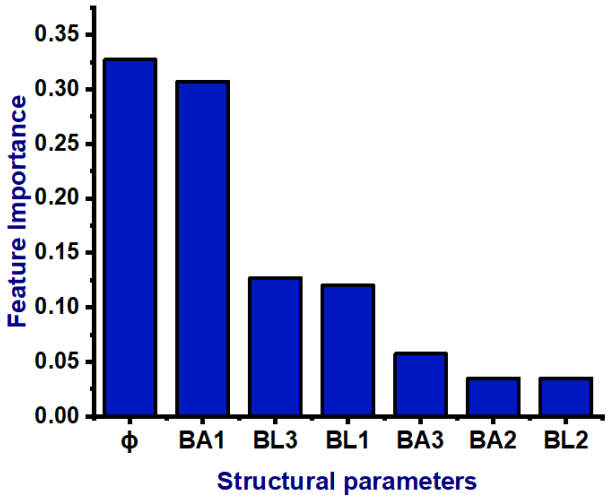

Figure 3. Feature Importance of all structural parameters for prediction of D (BA1 < BA2 < BA3, BL1 < BL2 < BL3)

Many machine learning algorithms, especially neural networks, are often seen as opaque, making their predictions hard to interpret. They learn complex functions from input and output data. In contrast, the GB model stands out. Alongside its impressive prediction accuracy, it inherently quantifies feature importance in decision-making, as illustrated in Figure 3. This reveals the significance of the seven descriptors. Notably, ϕ and small bond angle (BA1) emerge as the most influential in predicting D's sign, consistent with ϕ's correlation with D's magnitude. Following ϕ and BA1, BL3 and BL1 also show substantial importance. We selected four key parameters (ϕ, BA1, BL3, and BL1) from the seven structural descriptors to predict D's magnitude, achieving a remarkable test accuracy of 85%. GB provides an elegant solution to a challenge traditionally hard to quantify. We also explored the influence of the number of descriptors on prediction performance.

Prediction of E/D, g-factor

In addition to ZFS (D), the orientation of the magnetic field plays a vital role in the interaction with the magnetic moment, defined by the principal g-factors (g_X, g_Y, and g_Z), contributing to magnetic anisotropy. While structural parameters don't directly correlate with the g-tensor (Figure 5), the GB model predicts g-tensor values based on these parameters. Prediction accuracies for gx, gy, and gz reached 67%, 75%, and 72% with structural parameters alone, and improved to 74%, 80%, and 80% when E/D values were included (see Figure S3). The E parameter in the zero-field splitting tensor signifies the deviation from axial symmetry, reflecting the asymmetry in the electronic environment. A comprehensive understanding of E is pivotal for interpreting magnetic properties. The integration of machine learning (ML) to predict E from structural parameters enhances efficiency in evaluating anisotropic characteristics, expediting material design. This synergy offers insights into electronic and structural influences on magnetic behaviors. The predictive accuracy of E/D from structural parameters reached 73%, notably improving to 88% with the inclusion of g-tensor values. This underscores the reciprocal influence between the g-tensor and E/D, emphasizing their interconnected role in determining magnetic properties.

Classification of sign of D

For the classification purpose we trained nine machine learning models exclusively utilizing structural parameters. These models encompassed Logistic Regression (LR), k-Nearest

Neighbors (KNN), Support Vector Machine (SVM), Decision Tree (DT), Random Forests (RF), Adaptive Boosting (AD), Gradient Boosting (GB), and Multilayer Perceptron (MLP). The training process involved a 5-fold GridSearchCV with a grid-search cross-validation approach. The resulting hyperparameters from a single trial are consolidated in Table S5. The evaluation of these models encompassed various performance metrics, including accuracy, precision, recall, F1 score, and ROC curves, compared against ground truth data (detailed in Table S6). While each model offers distinct advantages, such as high accuracy or interpretability, our focus was on identifying a model with a balance of both. The results, depicted in Figure S4 and Table S6, revealed that all eight models achieved accuracy levels exceeding 80% and F1 scores surpassing 80%, with GB standing out at 95% accuracy and an average F1 score of 96%.

We performed a thorough comparative analysis of four key models, including GB, in addition to SVM, RF, and MLP. The ROC curve, showcased in Figure S5a, provides a visual representation of the relationship between the true positive rate (TPR) and false positive rate (FPR). It serves as a vital tool for assessing machine learning model performance, considering prediction uncertainty. A pronounced deviation of the ROC curve toward the top-left corner, away from the random guessing baseline (grey dashed line), signifies enhanced prediction accuracy. GB distinctly outperforms SVM, RF, and MLP, with the most substantial deviation, indicating superior accuracy. The Area Under the Curve (AUC) quantifies this performance and places GB at the forefront with an AUC of 0.94 surpassing SVM (0.92), RF (0.91), and MLP (0.90). Further evaluation using precision-recall (PR) curves in Figure 2c reveals GB's precision of 0.96 at a recall of 0.96, significantly outperforming SVM (0.94), RF (0.94), and MLP (0.94) at the same recall level. The confusion matrix underscores GB's superior recall of 0.95, surpassing SVM (0.79), RF (0.90), and MLP (0.8), indicating a higher number of accurate positive predictions.

To enhance our chemical understanding, we developed a flowchart based on the GB model, depicted in Figure 4. It illustrates the decision-making process for classifying sign of D based on the input structural parameters. Initially, the tree branches into two paths based on the value of ϕ: a left branch with $\phi < 0.2$ and a right branch with $\phi \geq 0.2$. Within the right branch, the determination of D's sign depends on the small L – Co – L bond angle. However, for small L – Co – L bond angles $\geq 107.8^{o}$, further division occurs based on the large L – Co – L bond angle, where $\geq 134^{o}$ tends to result in a negative D sign, and $< 134^{o}$ tends to yield a positive D sign. Conversely, within the right branch for L – Co – L bond angles $< 107.8^{o}$, subdivision is based on

the small Co – L bond length, with ≥1.96 Å typically indicating a positive D sign, while <1.96 Å often leads to a negative D sign. On the left branch with ϕ <0.2 Å, further division is determined by the small Co –L bond length. When the Co – L bond length is ≥1.95 Å and the small L – Co – L bond angle is <120°, a positive D sign is expected, whereas when the angle is ≥120°, a negative D sign is more likely. For Co – L bond lengths <1.95 Å and large Co – L bond lengths ≥2 Å, a negative D sign is typical, while <2 Å tends to correspond to a positive D sign. In summary, this decision tree provides a systematic and structured approach to deducing the sign of the parameter D by considering a range of critical structural parameters. It enhances our understanding of the magnetic behavior of the molecular systems studied, making it a valuable tool for researchers in the field.

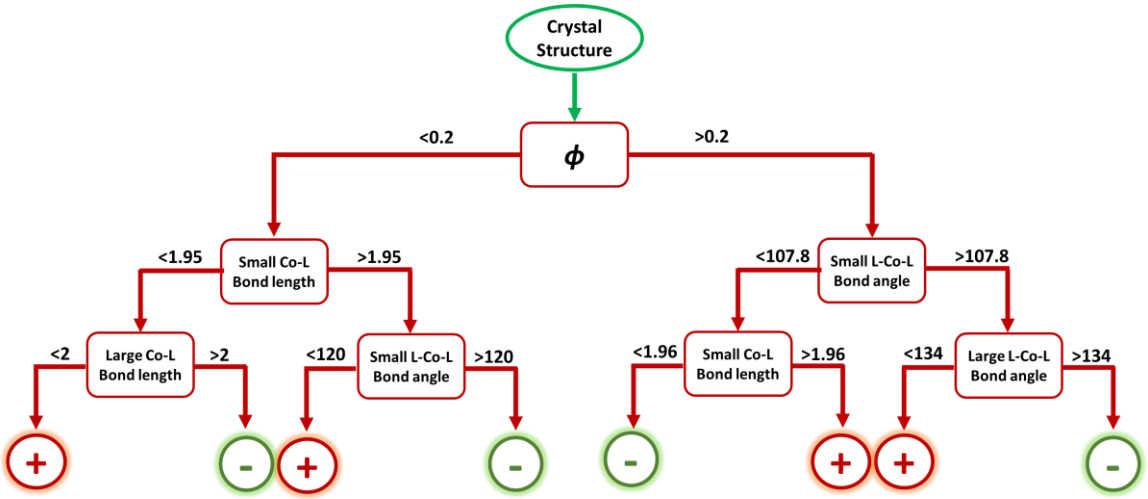

Figure 4. Visualization of a decision tree from the GB model for classifying sign of

In Figure5, we show a heat map that depicts the statistical correlation in our dataset. For generating the heat map, various structural parameters were considered, refined and developed. Further, two more parameters based on geometries were developed, the parameter ϕ (root-mean-square displacement (RMSD) of atomic coordinates from an ideal $\{CoN_3\}$ core possessing C_{3v} point group; see ESI for details)[45]. Among all the parameters tested, the ϕ parameter was found to be strongly correlated to the sign and strength of D values across all complexes. The ϕ has a high negative correlation (– 0.76) with the magnitude of D value and a moderately high correlation (– 0.59) with the sign of the D values. This indicates that even a slight modification in ϕ can result in a substantial alteration in both the magnitude and sign of the D value. For instance, for complex 128 (having the largest D), the value of ϕ is found to be 0.54.

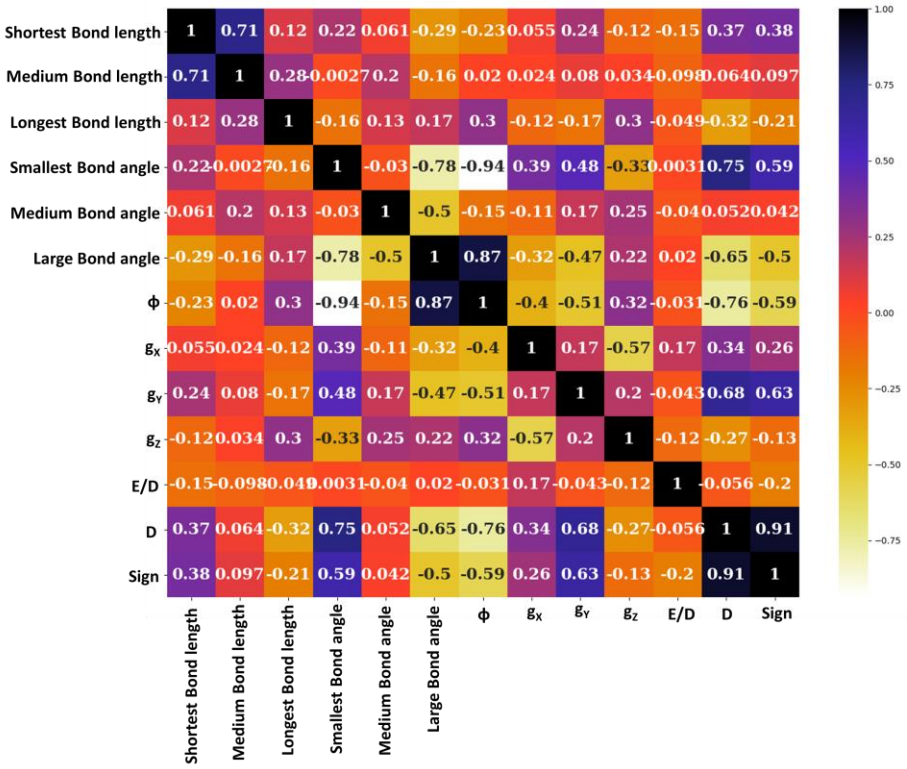

Figure 5. Heat map capturing the pairwise statistical correlation in the dataset.

The heatmap illustrates a clear relationship between ϕ and L-Co-L bond angles. Our dataset shows that as the bond angle deviates from 120°, ϕ increases; conversely, it decreases when the angle approaches 120°. This trend is evident, with medium bond angles showing weaker correlation, suggesting greater deviations from 120° contribute to molecular anisotropy. Analysis of the heat map reveals several interesting correlations. Specifically, it is evident that the parameter E/D shows little correlation with both D and the sign of D. On the other hand, the g_z value exhibits a strong positive correlation (0.69) with the magnitude of D, while the g_x and g_y values display negative correlations. This indicates that an increase in the g_z value corresponds to an increase in the magnitude of D, and vice versa. Conversely, increasing g_x and g_y values are associated with a decrease in the magnitude of D.

In conclusion, the study delves into the promising avenue of Single Molecule Magnets (SMMs) as potential alternatives to bulk nanomagnetic materials, particularly focusing on first-row transition metal-ion-based single-ion magnets (SIMs), notably those involving cobalt ions due to their favorable characteristics. The investigation emphasizes the importance of understanding magnetic anisotropy parameters, such as the axial zero-field splitting (D),

rhombic anisotropy (E/D), and principal g-factors (gx, gy, gz), in determining the performance of SIMs. Through the utilization of machine learning (ML) techniques, particularly Gradient Boosting Regression (GBR) and other models, the study successfully predicts these parameters with high accuracy, leveraging a comprehensive dataset of 627 molecules. Structural parameters, including bond lengths and angles, emerge as crucial predictors, with the GBR model demonstrating exceptional performance in predicting D values, achieving a minimal mean absolute error (MAE) of approximately 17 cm^{-1}. Additionally, ML algorithms excel in classifying the sign of D, with accuracy levels exceeding 95%. These findings underscore the potential of ML in advancing the understanding and design of novel single-ion magnets, offering valuable insights into their magnetic behavior and paving the way for future developments in molecular magnetism.

Computational Details

The *ab initio* calculations have been performed using the ORCA 5.0.4.[51] program to look into the zero-field splitting and anisotropic parameters. The scalar relativistic effect has been taken into account by using the Douglas-Kroll-Hess Hamiltonian.[52] DKH-contracted type basis set has been used for all the atoms, with DKH-def2-TZVP for Co and the atoms which are directly coordinated to the metal centre, for Si and N when it is not directly coordinated to metal DKH-def2-TZVP(-f), and DKH-def2-SVP for the rest of the atoms has been used.[53] Using the state-averaged complete active space self-consistent field (SA-CASSCF)[54,55] methods, for Co(II), seven electrons in five active orbitals have been taken into consideration, with 10 quartet and 40 doublet roots. Strongly contracted *N*-electron valence perturbation theory second-order (NEVPT2)[56] calculations have also been performed on top of the converged SA-CASSCF wave function to include the dynamic electron correlation. Spin-orbit interaction was accounted for with the quasi-degenerate perturbation theory (QDPT) approach using the spin-orbit mean-field (SOMF)[57] operator. Only spin-orbit contributions toward *zfs* were computed, and the Spin Hamiltonian (S.H.) parameters were determined from the Effective Hamiltonian Approach (EHA) formalism.[58] *Ab initio* ligand field theory (AILFT) analysis has also been carried out to obtain very accurate *d*-orbital energies of the studied complexes.

For the Co-SSS and Co-PPP model complexes, the optimisation has been performed using Gaussian 16.C[59] program with density functional calculations with uB3LYP functional.[60,61] For the Co centre TZVP level of basis set, for P and S, 6-311g(d,p) and for the rest of the atoms, 6-31G* has been used.[62]

Supporting Information

Detailed results of the calculations, Tables and all the supporting plots has been provided.

References

1 Zabala-Lekuona, A., Seco, J. M. & Colacio, E. Single-Molecule Magnets: From Mn12-ac to dysprosium metallocenes, a travel in time. *Coord. Chem. Rev.* **441**, 213984 (2021).

2 Christou, G., Gatteschi, D., Hendrickson, D. N. & Sessoli, R. Single-molecule magnets. *Mrs Bulletin* **25**, 66-71 (2000).

3 Coronado, E. Molecular magnetism: from chemical design to spin control in molecules, materials and devices. *Nat. Rev. Mater.* **5**, 87-104 (2020).

4 Frost, J. M., Harriman, K. L. & Murugesu, M. The rise of 3-d single-ion magnets in molecular magnetism: towards materials from molecules? *Chem. Sci.* **7**, 2470-2491 (2016).

5 Gomez-Coca, S., Cremades, E., Aliaga-Alcalde, N. & Ruiz, E. Mononuclear single-molecule magnets: tailoring the magnetic anisotropy of first-row transition-metal complexes. *J. Am. Chem. Soc.* **135**, 7010-7018 (2013).

6 Atanasov, M. *et al.* First principles approach to the electronic structure, magnetic anisotropy and spin relaxation in mononuclear 3d-transition metal single molecule magnets. *Coord. Chem. Rev.* **289**, 177-214 (2015).

7 Neese, F. & Pantazis, D. A. What is not required to make a single molecule magnet. *Faraday Discuss.* **148**, 229-238 (2011).

8 Ruiz, E. *et al.* Can large magnetic anisotropy and high spin really coexist? *Chem. Comm.*, 52-54 (2008).

9 Bunting, P. C. *et al.* A linear cobalt (II) complex with maximal orbital angular momentum from a non-Aufbau ground state. *Science* **362**, eaat7319 (2018).

10 Craig, G. A. *et al.* Probing the origin of the giant magnetic anisotropy in trigonal bipyramidal Ni (II) under high pressure. *Chem. Sci.* **9**, 1551-1559 (2018).

11 Zadrozny, J. M. *et al.* Magnetic blocking in a linear iron (I) complex. *Nat. Chem* **5**, 577-581 (2013).

12 Ruamps, R. *et al.* Giant ising-type magnetic anisotropy in trigonal bipyramidal Ni (II) complexes: experiment and theory. *J. Am. Chem. Soc.* **135**, 3017-3026 (2013).

13 Rau, I. G. *et al.* Reaching the magnetic anisotropy limit of a 3 d metal atom. *Science* **344**, 988-992 (2014).

14 Sarkar, A., Dey, S. & Rajaraman, G. Role of Coordination Number and Geometry in Controlling the Magnetic Anisotropy in FeII, CoII, and NiII Single‐Ion Magnets. *Chem. Eur. J.* **26**, 14036-14058 (2020).

15 Chibotaru, L. F. Theoretical understanding of anisotropy in molecular nanomagnets. *Molecular Nanomagnets and Related Phenomena*, 185-229 (2015).

16 Wang, C., Meng, Y.-S., Jiang, S.-D., Wang, B.-W. & Gao, S. Approaching the uniaxiality of magnetic anisotropy in single-molecule magnets. *Science China Chemistry* **66**, 683-702 (2023).

17 Wu, X., Li, J.-F. & Yin, B. The interpretation and prediction of lanthanide single-ion magnets from ab initio electronic structure calculation: the capability and limit. *Dalton Trans.* **51**, 14793-14816 (2022).

18 Kubica, A., Kowalewski, J., Kruk, D. & Odelius, M. Zero-field splitting in nickel (II) complexes: A comparison of DFT and multi-configurational wavefunction calculations. *J. Chem. Phys.* **138** (2013).

19 Ferbinteanu, M. *et al.* On the density functional theory treatment of lanthanide coordination compounds: a comparative study in a series of Cu–Ln (Ln= Gd, Tb, Lu) binuclear complexes. *Inorg. Chem.* **56**, 9474-9485 (2017).

20 Goodfellow, I., Bengio, Y. & Courville, A. *Deep learning*. (MIT press, 2016).

21 Lunghi, A. & Sanvito, S. Computational design of magnetic molecules and their environment using quantum chemistry, machine learning and multiscale simulations. *Nat. Rev. Chem.* **6**, 761-781 (2022).

22 Elton, D. C., Boukouvalas, Z., Butrico, M. S., Fuge, M. D. & Chung, P. W. Applying machine learning techniques to predict the properties of energetic materials. *Sci. Rep.* **8**, 9059 (2018).

23 Dou, B. *et al.* Machine learning methods for small data challenges in molecular science. *Chem. Rev.* **123**, 8736-8780 (2023).

24 Lunghi, A. & Sanvito, S. A unified picture of the covalent bond within quantum-accurate force fields: From organic molecules to metallic complexes' reactivity. *Sci. Adv.* **5**, eaaw2210 (2019).
25 Yu, H. *et al.* Complex spin Hamiltonian represented by an artificial neural network. *Phys. Rev. B* **105**, 174422 (2022).
26 Carleo, G. & Troyer, M. Solving the quantum many-body problem with artificial neural networks. *Science* **355**, 602-606 (2017).
27 Nguyen, V. H. A. & Lunghi, A. Predicting tensorial molecular properties with equivariant machine learning models. *Phys. Rev. B* **105**, 165131 (2022).
28 Lunghi, A. & Sanvito, S. Surfing multiple conformation-property landscapes via machine learning: Designing single-ion magnetic anisotropy. *J. Phys. Chem. C* **124**, 5802-5806 (2020).
29 Zaverkin, V., Netz, J., Zills, F., Köhn, A. & Kästner, J. Thermally averaged magnetic anisotropy tensors via machine learning based on Gaussian moments. *J. Chem. Theory Comput.* **18**, 1-12 (2021).
30 Novikov, I., Grabowski, B., Körmann, F. & Shapeev, A. Magnetic Moment Tensor Potentials for collinear spin-polarized materials reproduce different magnetic states of bcc Fe. *Npj Comput. Mater.* **8**, 13 (2022).
31 Gómez-Coca, S. *et al.* Origin of slow magnetic relaxation in Kramers ions with non-uniaxial anisotropy. *Nat. Commun* **5**, 4300 (2014).
32 Ruamps, R. *et al.* Ising-type magnetic anisotropy and single molecule magnet behaviour in mononuclear trigonal bipyramidal Co (II) complexes. *Chemical Science* **5**, 3418-3424 (2014).
33 Schneider, J. E., Goetz, M. K. & Anderson, J. S. Statistical analysis of C–H activation by oxo complexes supports diverse thermodynamic control over reactivity. *Chem. Sci.* **12**, 4173-4183 (2021).
34 Taylor, M. G. *et al.* Seeing is believing: Experimental spin states from machine learning model structure predictions. *J. Phys. Chem. A* **124**, 3286-3299 (2020).
35 Ren, S. *et al.* Ligand optimization of exchange interaction in Co (II) dimer single molecule magnet by machine learning. *J. Phys. Chem. A* **126**, 529-535 (2022).
36 Janet, J. P., Chan, L. & Kulik, H. J. Accelerating chemical discovery with machine learning: simulated evolution of spin crossover complexes with an artificial neural network. *J. Phys. Chem. Lett.* **9**, 1064-1071 (2018).
37 Janet, J. P. & Kulik, H. J. Predicting electronic structure properties of transition metal complexes with neural networks. *Chem. Sci.* **8**, 5137-5152 (2017).
38 Yao, X.-N. *et al.* Two-coordinate Co (II) imido complexes as outstanding single-molecule magnets. *J. Am. Chem. Soc.* **139**, 373-380 (2017).
39 Meng, Y.-S. *et al.* Observation of the single-ion magnet behavior of d 8 ions on two-coordinate Co (I)–NHC complexes. *Chem. Sci.* **6**, 7156-7162 (2015).
40 Deng, Y.-F., Han, T., Yin, B. & Zheng, Y.-Z. On balancing the QTM and the direct relaxation processes in single-ion magnets–the importance of symmetry control. *Inorg. Chem. Front.* **4**, 1141-1148 (2017).
41 Das, C., Rasamsetty, A., Tripathi, S. & Shanmugam, M. Magnetization relaxation dynamics of a rare coordinatively unsaturated Co (ii) complex: experimental and theoretical insights. *Chem. Comm.* **56**, 13397-13400 (2020).
42 Buitinck, L. *et al.* API design for machine learning software: experiences from the scikit-learn project. *arXiv preprint arXiv:1309.0238* (2013).
43 Schultz, C., Alegría, A. C., Cornelis, J. & Sahli, H. Comparison of spatial and aspatial logistic regression models for landmine risk mapping. *Appl Geogr* . **66**, 52-63 (2016).
44 Cover, T. & Hart, P. Nearest neighbor pattern classification. *IEEE Trans. Inf. Theory.* **13**, 21-27 (1967).
45 Burges, C. J. A tutorial on support vector machines for pattern recognition. *Data Min Knowl Discov* **2**, 121-167 (1998).
46 Ture, M., Tokatli, F. & Kurt, I. Using Kaplan–Meier analysis together with decision tree methods (C&RT, CHAID, QUEST, C4. 5 and ID3) in determining recurrence-free survival of breast cancer patients. *Expert Syst. Appl.* **36**, 2017-2026 (2009).
47 Pedregosa, F. *et al.* Scikit-learn: Machine learning in Python. *J Mach Learn Res* **12**, 2825-2830 (2011).
48 Freund, Y., Schapire, R. & Abe, N. A short introduction to boosting. *Jpn Soc Artif Intell* **14**, 1612 (1999).
49 Chen, T. & Guestrin, C. in *Proceedings of the 22nd acm sigkdd international conference on knowledge discovery and data mining.* 785-794.
50 Jaeger, S., Fulle, S. & Turk, S. Mol2vec: unsupervised machine learning approach with chemical intuition. *J. Chem. Inf. Model.* **58**, 27-35 (2018).
51 Neese, F., Wennmohs, F., Becker, U. & Riplinger, C. The ORCA quantum chemistry program package. *J. Chem. Phys.* **152**, 224108 (2020).
52 Weigend, F. Accurate Coulomb-fitting basis sets for H to Rn. *Phys. Chem. Chem. Phys.* **8**, 1057-1065 (2006).

53 Snyder Jr, J. W., Parrish, R. M. & Martínez, T. J. α-CASSCF: An efficient, empirical correction for SA-CASSCF to closely approximate MS-CASPT2 potential energy surfaces. *The journal of physical chemistry letters* **8**, 2432-2437 (2017).
54 Slavíček, P. & Martínez, T. J. Ab initio floating occupation molecular orbital-complete active space configuration interaction: An efficient approximation to CASSCF. *J. Chem. Phys.* **132**, 234102 (2010).
55 Guo, Y., Sivalingam, K. & Neese, F. Approximations of density matrices in N-electron valence state second-order perturbation theory (NEVPT2). I. Revisiting the NEVPT2 construction. *J. Chem. Phys.* **154**, 214111 (2021).
56 Park, J. W. Analytical gradient theory for quasidegenerate N-electron valence state perturbation theory (QD-NEVPT2). *J. Chem. Theory Comput.* **16**, 326-339 (2019).
57 Neese, F. & Solomon, E. I. Interpretation and Calculation of Spin‐Hamiltonian Parameters in Transition Metal Complexes. *J. Magn. Magn. Mater.*, 345-466 (2001).
58 Gaussian09, G. Inc. *Wallingford CT* **121**, 150-166 (2009).
59 Kohn, W., Becke, A. D. & Parr, R. G. Density functional theory of electronic structure. *J. Phys. Chem.* **100**, 12974-12980 (1996).
60 Kruse, H., Goerigk, L. & Grimme, S. Why the standard B3LYP/6-31G* model chemistry should not be used in DFT calculations of molecular thermochemistry: understanding and correcting the problem. *J. Org. Chem.* **77**, 10824-10834 (2012).
61 Peintinger, M. F., Oliveira, D. V. & Bredow, T. Consistent Gaussian basis sets of triple‐zeta valence with polarization quality for solid‐state calculations. *J. Comput. Chem.* **34**, 451-459 (2013).
62 Hutter, J., Iannuzzi, M., Schiffmann, F. & VandeVondele, J. cp2k: atomistic simulations of condensed matter systems. *Wiley Interdiscip. Rev. Comput. Mol. Sci.* **4**, 15-25 (2014).